THE JOURNAL OF PHYSICAL CHEMISTRY B

Article

Cite This: J. Phys. Chem. B 2019, 123, 4425−4433

pubs.acs.org/JPCB

Hydrogen Bond Networks in Binary Mixtures of Water and Organic Solvents

Simon Stehle[†,‡] and Andreas Siegfried Braeuer*[,†]

[†]Institute of Thermal-, Environmental- and Resources' Process Engineering (ITUN), Technische Universität Bergakademie Freiberg (TUBAF), Leipziger Strasse 28, 09599 Freiberg, Germany

[‡]Erlangen Graduate School in Advanced Optical Technologies (SAOT), Friedrich-Alexander-Universitaet Erlangen-Nuernberg (FAU), Paul-Gordan-Straße 6, 91052 Erlangen, Germany

Supporting Information

ABSTRACT: We here present an approach for the optical in situ characterization of hydrogen bond networks (HBNs) in binary mixtures of water and organic solvents (OSs), such as methanol, ethanol, and acetonitrile. HBNs are characterized based on (i) the analysis of experimental molar Raman spectra of the mixture, (ii) partial molar Raman spectra of the mixture constituents, and (iii) computed ideal molar Raman spectra of the mixture. Especially, the consideration of the partial molar Raman spectra provides insights into the development of hydrogen bonds of molecules of one species with their neighbors. The obtained Raman spectra are evaluated with respect to the centroid of the symmetric stretching vibration Raman signal of water and to the hydroxyl stretching vibration of alcohols. We show the influence of composition and temperature on the development of the HBN of the mixtures, the HBN of water, and the HBN of the OS molecules.

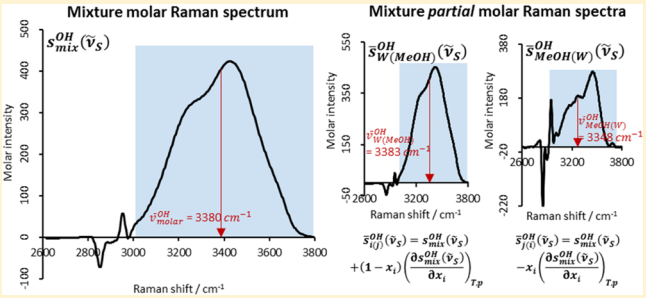

1. INTRODUCTION

Binary mixtures of water and an organic solvent (OS) such as acetonitrile (Acn), methanol, or ethanol are miscible in a single liquid and transparent phase over the entire composition range at moderate temperature and pressure. These binary mixtures have in common that their electrical conductivity, permittivity, specific volume, enthalpy of mixing, or scattering behavior exhibit a non-monotonic behavior when regarded as a function of the composition of the mixture. A controversial discussion on the origin of this non-monotonic behavior has grown over the last 70 years and still theories of the intermolecular interactions in these mixtures are ambiguous. As the "organic solvent" contains a hydrophobic part, the terms "hydrophobic solvation" or "hydrophobic effects" can summarize all the subsequently mentioned theories.

The most debated theory is the so called "iceberg theory" from Frank and Evans who discussed in 1945 entropic anomalies in several water diluted binary mixtures.[1] They have chosen the term iceberg because they proposed that water molecules surrounding a strong diluted hydrophobic or amphiphile compound create a stronger hydrogen bond network (HBN) with their water neighbors—like in ice—than those in bulk water. Later, in accordance with the hydration of salt ions dissolved in water, the term "hydrophobic hydration" was common[2−5] in order to describe the development of "hydrate-like" or "ice-like" formations of water molecules.[6] This concept was confirmed[2,7−11] but also challenged[12−16] by experimental and theoretical investigations. However, the formation of water molecules in these mixtures is under discussion. For example, other theories about the development of

- an incomplete mixing on a molecular scale,[13,17,18]
- water diluted mixtures without strengthening the structure of water,[19−22]
- a stronger network between the water molecules surrounding a hydrophobic/amphiphile molecule,[4,9,11,14,23−29]
- hydration shells around single or few hydrophobic/amphiphile molecules,[30,31]
- hydrophobic/amphiphile clusters at low concentration of the hydrophobic/amphiphile compound,[4,14,19,22−24,30,32,33]
- water clusters at low water concentration,[13,22,30,34−36]
- greater percolating networks of water and the hydrophobic/amphiphile compound with equimolar compositions,[15,20,22,27,37−41]
- hydrophilic and hydrophobic/amphiphile clusters over a broad composition range,[42−44] and
- a complete and homogeneous mixing over a defined composition range[28,31,32]

Received: March 26, 2019
Revised: April 26, 2019
Published: May 2, 2019

DOI: 10.1021/acs.jpcb.9b02829
J. Phys. Chem. B 2019, 123, 4425−4433

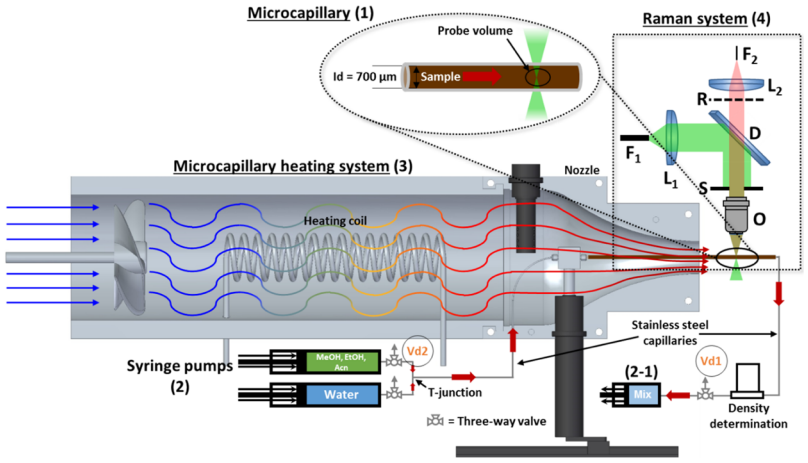

Figure 1. Schematic of the experimental setup (1-3) and the Raman system (4); $L_{1,2}$: convex lenses; O: microscope objective; D: dichroic mirror; $F_{1,2}$: optical fibers; R: long pass filter (535 nm); S: slit.

contribute to the current debate. This incomplete above listed abstract of the debate about liquid binary water/alcohol and water/nitrile mixtures shows the dispute and challenging task to draw a complete and coherent picture from the comprehensive results stemming from thermodynamic studies, molecular dynamic simulations, and a variety of measurement techniques.

Common to the systems analyzed in the above listed studies is that their molecular formation and the dominant intermolecular forces are strongly influenced by the development of a HBN. The unique ability of water to form as many hydrogen (H)-bonds as covalent bonds per molecule[45] is supposed to be one reason for the abnormalities observed in these mixtures. As the intermolecular H-bonds affect the intramolecular covalent bonds of water and alcohols, spectroscopic analysis of the intramolecular covalent bond vibrations is—besides thermodynamic and theoretical studies—often used to investigate the intramolecular HBN of the mixture. In this context, infrared (IR) absorption is one frequently applied spectroscopic technique. For example, Takamuku et al. investigated water/Acn mixtures over the whole composition range with X-ray diffraction and IR spectroscopy.[29] At Acn molar fractions of $x_{Acn} < 0.6$, the "X-ray radial distribution functions and IR spectra suggested that the HBN of water is enhanced". Furthermore, within the composition range $0.2 < x_{Acn} < 0.6$, they observed micro-heterogeneity with coexisting water and Acn clusters. They supposed that clustering is an explanation for the maximum of the enthalpy of mixing at $x_{Acn} = 0.6$. Many other examples of the application of IR spectroscopy can be found in the literature.[20,21,46−50]

Raman spectroscopy is an alternative and also frequently applied technique for the investigation of the HBN.[7,11,31,38,51−53] In 2012, Lin et al. evaluated polarized Raman spectra from different water/alcohol mixtures (methanol, ethanol, 1-propanol, and *n*-propanol) over the whole composition range.[31] The stronger the intermolecular interactions are, the slower the translational motions that can be deduced from the Raman spectra. They observed a sharp increase in the translational relaxation time during the addition of small amounts of alcohol to water and interpreted this with the development of water hydration shells around the alcohol molecules. In the water rich regime, they interpreted this as a confirmation for the "iceberg model".

In contrast to the majority of previous Raman investigations, we here do not analyze the Raman spectrum of the mixture as a whole, but separate the shares originating from each species in the mixture. This makes possible the extraction of information about the involvement of each species in the HBN in the mixture. The information about the development of the HBN is deduced from the symmetric stretching vibration of water and from the OH stretching vibration of alcohols. Unfortunately, both Raman signatures completely overlap in the spectral range of Raman shifts between 3000 and 3800 cm^{-1}. Therefore, we introduce a method for the efficient separation of the two overlapping Raman signatures that is based on the consideration of partial molar spectra. Finally, from the analysis of the partial molar spectra of each compound in the mixture, information about the role of this compound in the HBN can be gathered, while the analysis of the spectrum of the mixture provides information of the overall development of the HBN.

2. EXPERIMENTAL SECTION

2.1. Materials. Experiments were carried out with Acn (Merck LiChrosolv, purity > 99.9%, Germany), methanol (MeOH) (VWR HiPerSolv, purity > 99.8%, USA), ethanol (EtOH) (Merck Uvasol, purity > 99.9%, Germany), and distilled water (W) (KERNDL, conductivity < 10 $\mu S\ cm^{-1}$, Germany).

2.2. Experimental Setup. The binary mixtures were analyzed via Raman spectroscopy in a microcapillary setup (MCS) that according to Figure 1 consists of the microcapillary itself (1), three syringe pumps (2) and (2-1), a microcapillary heating system (3), and a Raman system (4).

The investigated compounds (water and OS) flow through the MCS from a starting point to the end, and wherefore the functionality of the MCS and the function of its components will be described along the flow direction. At the starting point, two of the three syringe pumps [(2) in Figure 1] (2× Teledyne Isco 100 DX, USA) one containing water and the other one containing either MeOH, EtOH, or Acn reduce their volumes to feed a specific volume flow ($\pm 1\ \mu L\ min^{-1}$) into the MCS. The three-way valves next to the outlets of the syringe pumps help refill/renew or clean the respective syringe pump. Within the subsequent T-junction, the two fed compounds merge and mix within a stainless steel capillary (ID = 1 mm,

DOI: 10.1021/acs.jpcb.9b02829
J. Phys. Chem. B 2019, 123, 4425−4433

length = 0.6 m) from which 0.25 m of it is located within the heating system area (3) to preheat the mixture before it reaches the fused silica microcapillary. The temperature conditioning of the binary mixture is assured by the microcapillary heating system (3). A fan channels air above a heating coil according to the simple principle of a hairdryer whereupon a nozzle guides the heated air laminar along the fused silica microcapillary [(1) in Figure 1]. A controller (JUMO, iTRON 32, Switzerland) that receives the actual temperature value from a temperature sensor located 5 mm beside the measuring volume automatically determines the heating power of the heating coil required for a certain temperature set point. The transition from the stainless steel capillary toward the fused silica microcapillary (ID = 700 μm, OD = 850 μm) (Molex, Polymicro Technologies) is sealed using a PEEK sleeve—located between the stainless steel capillary and the fused silica microcapillary—and two component glue. Further downstream, immediately after the transition from the microcapillary to a short stainless steel capillary, a Coriolis densitometer (Bronkhorst, Mini Cori-Flow ML120, Germany) determines the density and the mass flow of the mixture. The Coriolis densitometer is conditioned to exactly measure the temperature and the pressure of the fluid mixture in the measuring volume. The stainless steel capillary further connects the Coriolis densitometer with the third syringe pump [(2-1) in Figure 1] (Teledyne Isco 500 D). This pump runs reverse and takes up the binary mixture in a way that the desired pressure within the entire microcapillary path is constant. According to the maximal volume flow of the summation of all delivered compounds of 220 μL min^{-1} the maximal flow rate is 0.95 cm s^{-1} at the lowest inner diameter of the MCS. The pressure indications of the two feed pumps at the start point of the MCS and the one reverse running pump at the end point of the MCS do not show a measurable pressure drop along the MCS.

The Raman system [(4) in Figure 1], whereof the Raman sensor is sketched, includes also the excitation continuous wave diode pumped solid-state laser (Smaba, Cobolt, 531.93 nm, 0.250 W, Sweden) and a spectrometer for signal detection (QE Pro, Ocean Optics, 100 μm entrance slit, USA), including a cooled 1024 × 58 (pixels) charge coupled device detector. An optical fiber (F_1) guides the excitation laser beam toward the Raman sensor where the beam is collimated (L_1) and reflected through a high power microscope objective (High Power MicroSpot LMH-20×, ThorLabs, NA = 0.4, USA) (O) that focuses the excitation laser beam into the probe volume at the center of the microcapillary (C). The high NA of the microscope objective ensures that no signals from the microcapillary walls reach the spectrometer and interfere with the desired Raman signal of the fluids contained inside the capillary. An aperture before the objective (S) lets pass only the high intensity part of the laser beam with originally a Gaussian intensity profile. The red-shifted Raman signal scattered in the probe volume passes straight through the dichroitic mirror (reflecting wavelengths smaller than 535 nm and transmitting wavelengths larger than 535 nm) (D) whereon a razor edge long-pass filter (R) blocks the remaining elastically scattered light. The second lens (L_2: f = 60 mm and Ø = 25.4 mm; NA = 0.21) focuses the Raman signals into the detection fiber (core Ø = 200 μm) (F_2). The detection fiber guides the detected signals to the spectrometer.

2.3. Raman Spectra Acquisition Using MCS. At the beginning of each experimental run, we flush the system with pure liquid water at the desired temperature of 308, 318, or 328 K. Therefore, the first water containing syringe pump delivers 200 μL min^{-1} of water until the pressure within the third syringe pump at the end of the microcapillary reaches 0.4 MPa. Now, the third syringe pump starts to run reverse and takes up the fed water in a way that the pressure within the MCS remains constant at 0.4 MPa. We record the first Raman spectra from pure water at the set temperature that correspond to a mixture composition of the molar fraction x_W = 1. Afterward, the second syringe pump containing either Acn, EtOH, or MeOH starts delivering the compound into the MCS while at the same time the feed flow of the water is reduced accordingly. The two compounds mix at the T-junction and stream afterward through the stainless steel capillary in the heating system, before the mixture enters the fused silica microcapillary. Via the set flow rates of the two feed syringe pumps, the composition of the mixture inside the capillary system can be adjusted. For example, 152 μL min^{-1} ethanol and 47 μL min^{-1} water were set to achieve an equimolar binary mixture. The overall volumetric flow rate with respect to the summation of the pure substance water and solvent is maintained between 200 and 220 μL min^{-1}. The small flow velocities (less than 1 cm s^{-1}) assure that the fluids inside the capillary adopt the temperature of the air inside the heating system, before they pass the Raman measurement location. Gradually the composition of the binary mixture is varied from pure water x_W = 1 to pure OS x_W = 0. When the mixture is varied from one composition to the next one, it takes approximately 20 min to reach stationary conditions. Stationary conditions are first indicated by the stationary and non-fluctuating mixture density and mass flow (Coriolis) and second by a constant Raman spectrum. At the end of the experimental run, the MCS is flushed (200 μL min^{-1}) with the OS in order to record a pure OS spectrum x_W = 0. During the entire procedure, the mixture density and the mass flow are recorded (Coriolis). The density of the mixture is required to convert the molar compositions (mol mol^{-1}) of the mixture into concentrations (mol L^{-1}).

For each stationary mixture composition, 100 Raman spectra are recorded with an exposure time of 3.4 s spectrum^{-1}. Consequently, the acquisition of 100 Raman spectra takes ∼340 s per adjusted mixture composition. The Raman spectra are processed and evaluated with respect to the development of hydrogen bonds according to the procedure described in the section that follows.

3. DATA EVALUATION

3.1. Processing of the Spectra. The "OH stretching vibration" from now on refers to the symmetric stretching vibration of water and the OH stretching vibration of the hydroxyl functional group of alcohols. For every single analyzed mixture composition, a mean spectrum is averaged from the 100 Raman spectra. Each experiment was performed in triplicate, in total on three different days. The standard deviation of the triplication is provided as error bars in the figures that follow.

Figure 2 summarizes from the top to the bottom how the mean spectra were treated in order to determine (i) the experimental molar Raman spectra of the mixture and (ii) the partial molar Raman spectra of the mixture constituents. A detailed description of the chain of processing the spectra is provided in the Supporting Information. Here a short overview is given.

DOI: 10.1021/acs.jpcb.9b02829
J. Phys. Chem. B 2019, 123, 4425−4433

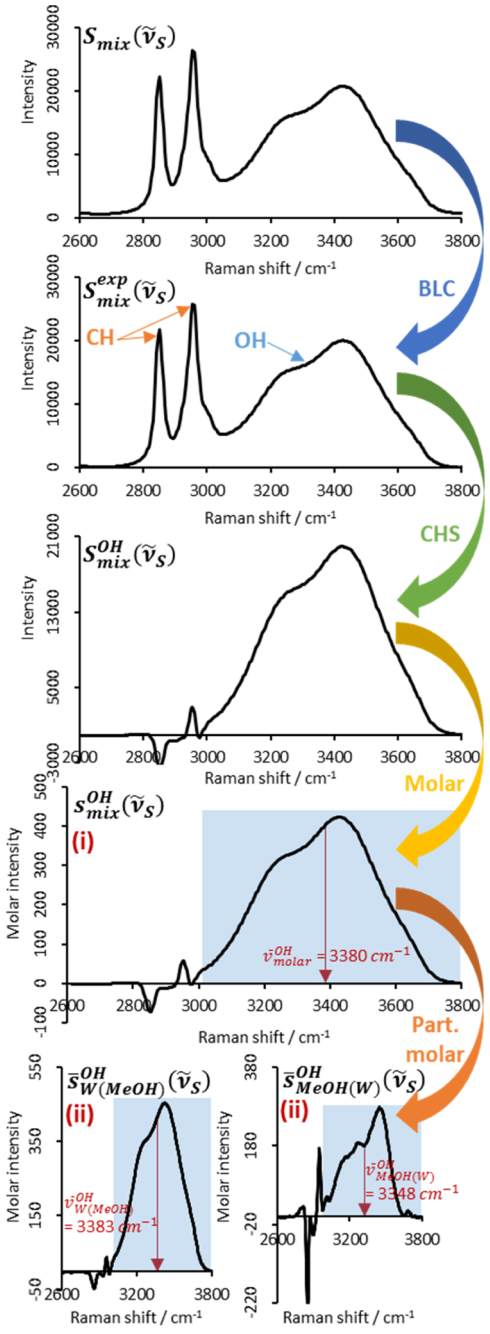

Figure 2. Raman spectra of an example W/MeOH mixture (x_W = 0.84) at 308 K and 0.4 MPa showing the Raman shift region of the CH- and OH stretching vibration. From the top to the bottom: pure spectrum as recorded $S_{mix}(\tilde{\nu}_S)$, spectrum after the baseline correction $S^{exp}_{mix}(\tilde{\nu}_S)$, isolated OH Raman spectrum $S^{OH}_{mix}(\tilde{\nu}_S)$ after the subtraction of the CH Raman spectrum (CHS), molar OH Raman spectrum $s^{OH}_{mix}(\tilde{\nu}_S)$, and partial molar OH Raman spectra of water $\bar{s}^{OH}_{W(MeOH)}(\tilde{\nu}_S)$ in MeOH and methanol $\bar{s}^{OH}_{MeOH(W)}(\tilde{\nu}_S)$ in water. The blue shaded rectangles mark the Raman shift region from which the centroid is calculated. A detailed description of the chain of processing the spectra is provided in the Supporting Information.

Figure 2 shows at the top the raw mean spectrum $S_{mix}(\tilde{\nu}_S)$ acquired from a water/methanol (W/MeOH) mixture (x_W = 0.84) as a function of the Raman shift $\tilde{\nu}_S$. The background is fitted using a cubic spline function and subtracted from $S_{mix}(\tilde{\nu}_S)$ in order to achieve a background compensated spectrum $S^{exp}_{mix}(\tilde{\nu}_S)$ that is shown as the second spectrum in Figure 2. The Raman spectral features that can be assigned to the CH vibration of the OSs and to the OH stretching vibration of water and alcohols are labelled "CH" or "OH", respectively. The CH Raman signatures are subtracted in order to obtain an isolated OH Raman spectrum $S^{OH}_{mix}(\tilde{\nu}_S)$ of the mixture, which is shown as the third spectrum in Figure 2. $S^{OH}_{mix}(\tilde{\nu}_S)$ (capital letter "S") is divided by the concentration (mol L^{-1}) of the mixture in order to obtain a molar Raman spectrum $s^{OH}_{mix}\tilde{\nu}_S)$ (lowercase letter "s") of the OH vibration of the mixture that is shown as the fourth spectrum in Figure 2. The concentration of the mixture is known from the density measurements (Coriolis), the molar masses, and the set composition. Finally, the molar Raman OH spectrum of the mixture is deconstructed (for details see the Supporting Information) into the shares assignable to water and the OS. As the construction method is identical to the determination of partial molar properties from molar mixture properties, the corresponding and resulting spectra shown in Figure 2 at the bottom are referred to as partial molar Raman spectra $\bar{s}^{OH}_{i(j)}(\tilde{\nu}_S)$ of the respective compound i in a mixture with compound j. For example, $\bar{s}^{OH}_{MeOH(W)}(\tilde{\nu}_S)$ shows the partial molar Raman spectrum of the OH vibration of MeOH in the mixture with water. $\bar{s}^{OH}_{W(MeOH)}(\tilde{\nu}_S)$ shows the partial molar Raman spectrum of the OH vibration of water in the mixture with MeOH. The partial molar Raman spectrum of i in j represents (exactly as partial molar thermodynamic properties do) how the molar Raman spectrum of the mixture changes if an infinite small amount of i is added to the mixture. The molar fraction weighted summation

$$s^{OH}_{W/MeOH}(\tilde{\nu}_S) = x_W \bar{s}^{OH}_{W(MeOH)}(\tilde{\nu}_S) + (1 - x_W)\bar{s}^{OH}_{MeOH(W)}(\tilde{\nu}_S) \quad (1)$$

of the partial molar spectra $\bar{s}^{OH}_{W(MeOH)}(\tilde{\nu}_S)$ and $\bar{s}^{OH}_{MeOH(W)}(\tilde{\nu}_S)$ is the molar spectrum of the mixture $s^{OH}_{W/MeOH}(\tilde{\nu}_S)$. According to authors' knowledge, the deconstruction of mixture spectra into their spectrally overlapping shares based on the computation of partial molar spectra is new.

Figure 3 shows for the example binary system W/MeOH, how the ideal molar mixture spectrum

$$s^{OH,ideal}_{W/MeOH}(\tilde{\nu}_S) = x_W s^{OH,0}_{W}(\tilde{\nu}_S) + (1 - x_W)s^{OH,0}_{MeOH}(\tilde{\nu}_S) \quad (2)$$

is computed from the molar Raman spectra of the pure (upper index 0) compounds $s^{OH,0}_{W}(\tilde{\nu}_S)$ and $s^{OH,0}_{MeOH}(\tilde{\nu}_S)$ as a molar fraction weighted average. Figure 3 also shows that the ideal spectrum $s^{OH,ideal}_{mix}(\tilde{\nu}_S)$ is different from the real molar spectrum of the mixture $s^{OH}_{mix}(\tilde{\nu}_S)$, exactly as it is the case for many thermodynamic properties, such as entropy or Gibbs energy. As it will be shown in the next section, the difference between the two OH spectra can be quantified based on the Raman shifts of their centroids. This is why the centroids are also indicated in Figures 2 and 3.

In Figures 2 and 3, the positive and negative zig-zag peaks between 2800 and 3000 cm^{-1} remain as a mathematical residue after the subtraction of the CH Raman signal. They do not have any physical meaning and they are not regarded in further processing of the data.

3.2. Determination of the Centroid of the OH Stretching Vibration Raman Signal. The Raman shift of the centroid $\bar{\nu}^{OH}$ (centroid position) of the OH stretching vibration is computed as generally described in ref 54

DOI: 10.1021/acs.jpcb.9b02829
J. Phys. Chem. B 2019, 123, 4425−4433

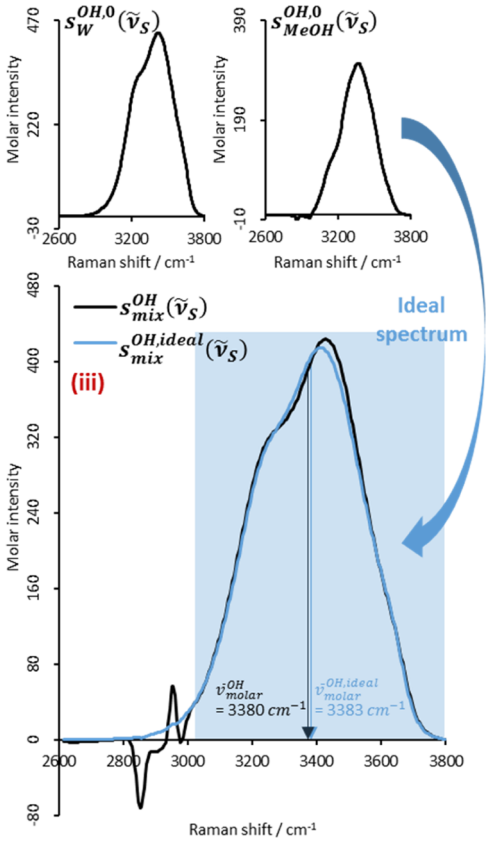

Figure 3. Isolated OH stretching vibration of the molar Raman spectra of pure water and pure methanol at 308 K and 0.4 MPa (upper row). Molar Raman spectra of the real (black) and ideal (blue) W/MeOH mixture at $x_W = 0.84$ (lower row). The blue shaded rectangle marks the Raman shift region from which the centroid is calculated.

$$\bar{\nu}^{OH} = \frac{1}{\int_{3033cm^{-1}}^{3798cm^{-1}} s(\tilde{\nu}_S)d\tilde{\nu}_S} \int_{3033cm^{-1}}^{3798cm^{-1}} s(\tilde{\nu}_S)\tilde{\nu}_S \, d\tilde{\nu}_S \quad (3)$$

- In eq 3, we consider the molar OH Raman spectrum of the mixture $s(\tilde{\nu}_S) = s^{OH}_{mix}(\tilde{\nu}_S)$ for the computation of its centroid position $\bar{\nu}^{OH} = \bar{\nu}^{OH}_{mix}$.
- We consider the partial molar spectra of the constituents of the mixture $s(\tilde{\nu}_S) = \bar{s}^{OH}_{i(j)}(\tilde{\nu}_S)$ for the computation of their centroid position $\bar{\nu}^{OH} = \bar{\nu}^{OH}_{i(j)}$.
- We consider the ideal molar mixture spectra $s(\tilde{\nu}_S) = s^{OH,ideal}_{mix}(\tilde{\nu}_S)$ for the computation of $\bar{\nu}^{OH} = \bar{\nu}^{OH,ideal}_{mix}$.

The calculation of the centroid of the OH stretching vibration is a straightforward method to observe and characterize changes in the shape of the OH stretching vibration that is affected by the average development of the HBN of the mixture. The stronger the HBN developed, the lower the energy stored in the OH vibration of alcohols and/or water and therefore smaller is the centroid position $\bar{\nu}^{OH}$.

4. RESULTS AND DISCUSSION

Figure 4 shows the centroid positions of the molar OH Raman spectra of the three binary mixtures water/methanol (W/MeOH), water/ethanol (W/EtOH), and water/Acn (W/Acn) as a function of the water molar fraction in the mixture x_W. The centroids $\bar{\nu}^{OH}_{molar}$ computed from the real mixture spectra $s^{OH}_{W/MeOH}(\tilde{\nu}_S)$, $s^{OH}_{W/EtOH}(\tilde{\nu}_S)$, and $s^{OH}_{W/Acn}(\tilde{\nu}_S)$ are given as solid discs, while the centroids $\bar{\nu}^{OH,ideal}_{mix}$ computed from the ideal mixture spectra $s^{OH,ideal}_{W/MeOH}(\tilde{\nu}_S)$, $s^{OH,ideal}_{W/EtOH}(\tilde{\nu}_S)$, and $s^{OH,ideal}_{W/Acn}(\tilde{\nu}_S)$ are given as black crosses. The very right values ($x_W = 1$) represent the centroid positions of the OH Raman spectrum of pure water and the very left values ($x_W = 0$) represent the centroid positions of the OH Raman spectrum of pure OSs. While the alcohols MeOH and EtOH feature an OH Raman signal, Acn—simply due to the lack of the hydroxyl group—does not feature an OH Raman signal. Therefore, no data points are given for pure Acn ($x_W = 0$). The Acn-richest W/Acn mixture, in which the OH Raman spectrum of water is still observable, is $x_W = 0.02$ (see the Supporting Information). Therefore, only in the case of W/Acn, the ideal mixture spectra $s^{OH,ideal}_{W/Acn}(\tilde{\nu}_S)$ were not computed according to eq 2 but according to

$$s^{OH,ideal}_{W/Acn}(\tilde{\nu}_S) = \frac{(x_W - 0.02)}{0.98} s^{OH,0}_{w}(\tilde{\nu}_S) + \frac{(1 - x_W)}{0.98} s^{OH,x_w=0.02}_{W/Acn}(\tilde{\nu}_S) \quad (4)$$

from the molar Raman spectrum of pure water $s^{OH,0}_{W}(\tilde{\nu}_S)$ and the molar Raman spectrum $s^{OH,x_w=0.02}_{W/Acn}(\tilde{\nu}_S)$ of the Acn-rich mixture with $x_W = 0.02$. The centroid positions were then computed as always according to eq 3.

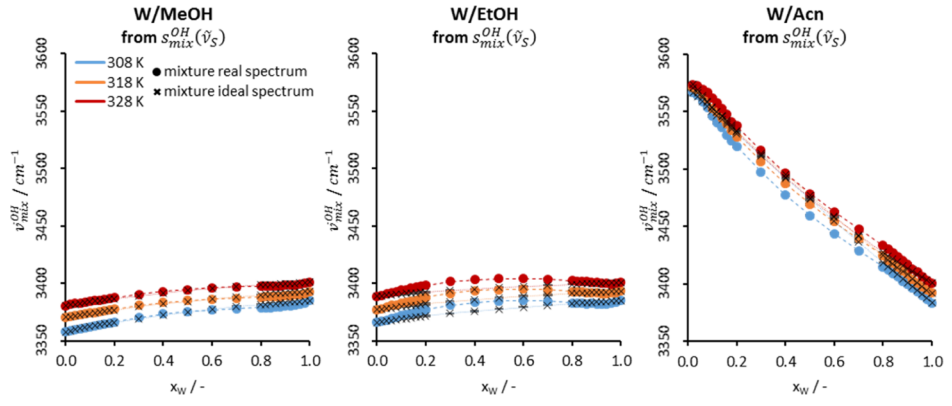

Figure 4. Centroid positions $\bar{\nu}^{OH}_{mix}$ of the molar spectra as a function of the mixture composition of the binary mixtures W/MeOH, W/EtOH, and W/Acn at 308, 318, and 328 K. The dashed lines are to guide the eyes and the error bars represent the standard deviation of the triplication of each data point (here smaller than the data points).

DOI: 10.1021/acs.jpcb.9b02829
J. Phys. Chem. B 2019, 123, 4425−4433

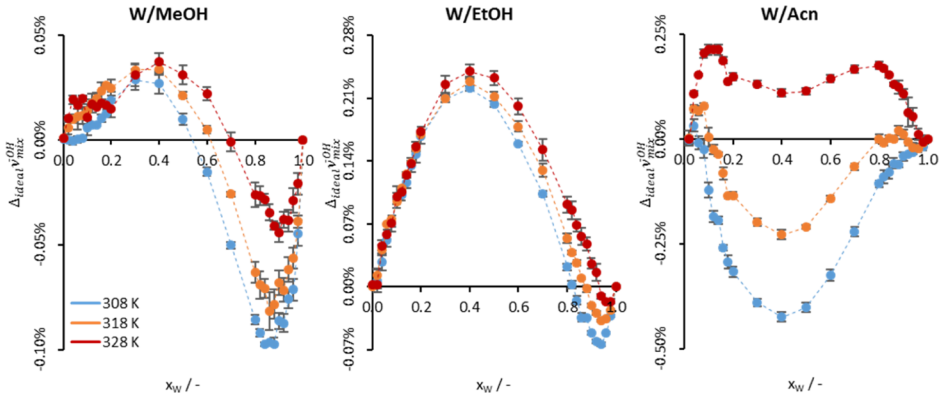

Figure 5. Relative deviations $\Delta_{ideal}\bar{\nu}^{OH}_{mix}$ of the real and ideal centroid positions as a function of the composition of the binary mixtures W/MeOH, W/EtOH, and W/Acn at 308, 318, and 328 K. The dashed lines are to guide the eyes and the error bars represent the standard deviation of the triplication of each data point.

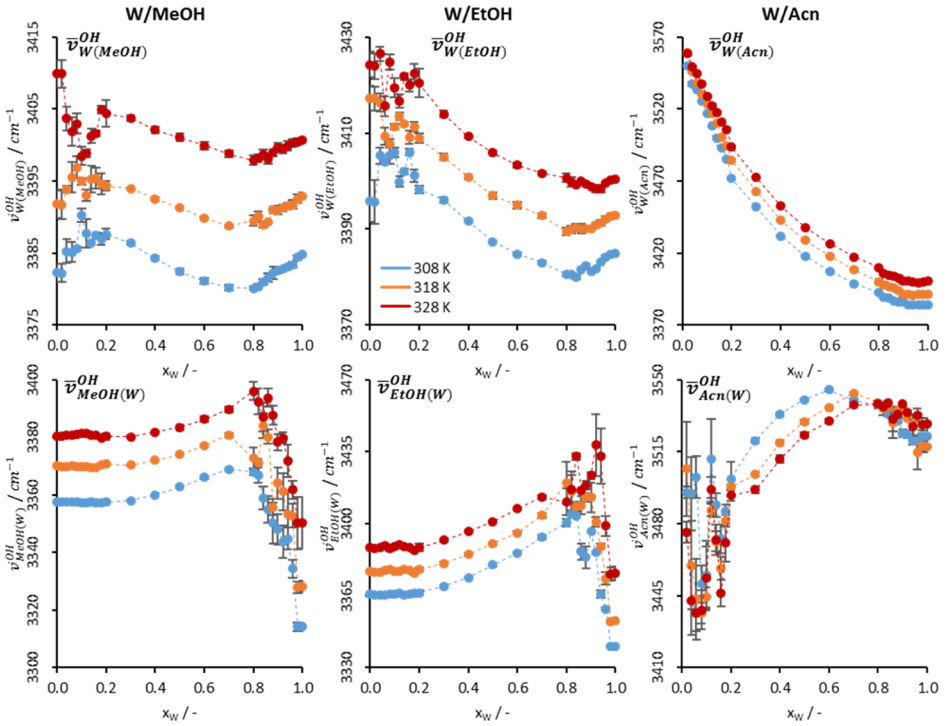

Figure 6. Centroid positions $\bar{\nu}^{OH}_{i(j)}$ and $\bar{\nu}^{OH}_{j(i)}$ of the partial molar Raman spectra $\bar{s}^{OH}_{i(j)}(\tilde{\nu}_S)$ and $\bar{s}^{OH}_{j(i)}(\tilde{\nu}_S)$, for the binary mixtures W/MeOH, W/EtOH, and W/Acn and at 308, 318, and 328 K as a function of the binary mixture composition x_w.

The centroid position $\bar{\nu}^{OH}_{mix}$ increases if water is diluted with Acn, but decreases when water is diluted with MeOH or EtOH. The addition of Acn to water weakens the HBN of the mixture in the entire composition range, while the HBN of the mixture is strengthened when MeOH or EtOH are added. The centroid positions $\bar{\nu}^{OH,ideal}_{mix}$ (black crosses) of the ideal molar OH Raman spectra $s^{OH,ideal}_{mix}(\tilde{\nu}_S)$ are close to the ones ($\bar{\nu}^{OH}_{mix}$) computed from the real molar OH Raman spectra $s^{OH}_{mix}(\tilde{\nu}_S)$ for every investigated mixture. With the increasing temperature, the HBN is less developed. Therefore $\bar{\nu}^{OH}_{mix}$ increases with the increasing temperature.

In order to quantify the deviation of the real $\bar{\nu}^{OH}_{mix}$ and the ideal $\bar{\nu}^{OH,ideal}_{mix}$ centroid positions, the relative deviations

$$\Delta_{ideal}\bar{\nu}^{OH}_{mix} = \frac{\bar{\nu}^{OH}_{mix} - \bar{\nu}^{OH,ideal}_{mix}}{\bar{\nu}^{OH,ideal}_{mix}} \quad (5)$$

for the three mixtures are provided as a function of the mixture composition at three different temperatures in Figure 5.

Here, negative values imply that the HBN represented by the mixture real spectrum is more developed than the HBN represented by the mixture ideal spectrum. Vice versa, positive values imply that the HBN shown by the mixture real spectrum is less developed than that by the ideal one. It should be underlined here that according to eq 2 the ideal molar OH Raman spectra $s^{OH,ideal}_{mix}(\tilde{\nu}_S)$ are simply computed as a molar fraction weighted average of the pure compound OH Raman spectra. Therefore, any decay of $\Delta_{ideal}\bar{\nu}^{OH}_{mix}$ from zero indicates that the HBN in the real mixture is not simply a weighted average of the HBN of the pure compounds but the result of a change in the intermolecular forces and of the orientation of the molecules relative to each other. Figure 5 shows that the negative deviations of $\Delta_{ideal}\bar{\nu}^{OH}_{mix}$ increase with decreasing temperature and that the positive deviations of $\Delta_{ideal}\bar{\nu}^{OH}_{mix}$

DOI: 10.1021/acs.jpcb.9b02829
J. Phys. Chem. B 2019, 123, 4425−4433

increase with increasing temperature. Therefore, cold temperatures support the formation of the HBN in real mixtures that are more intense than in ideal mixtures. Warm temperatures support the formation of the HBN that are less intense than in the ideal mixture case. The HBN deviations from the ideal mixture behavior can explain the anomalies found for the respective mixtures with respect to their density, conductivity, and other properties.[27,55−58] $\Delta_{ideal}\overline{\nu}^{OH}_{mix}$ was found to be most temperature sensitive for the system W/Acn. This can be explained by the proximity of the analyzed temperatures to the upper critical solution temperature of this binary system, which at ambient pressure is at 272 K.[59]

Figure 6 shows the centroid positions $\overline{\nu}^{OH}_{i(j)}$ and $\overline{\nu}^{OH}_{j(i)}$ of the partial molar Raman spectra $\overline{s}^{OH}_{i(j)}(\tilde{\nu}_S)$ and $\overline{s}^{OH}_{j(i)}(\tilde{\nu}_S)$, respectively, for all three analyzed mixtures in three columns and at all three analyzed temperatures as a function of the binary mixture composition x_w. The upper three diagrams show the centroid position of the partial molar Raman spectrum of water in the mixture with the OS and thus represent the development of the water-HBN in the mixture. In this context, water-HBN refers to the HBN that water molecules develop with their neighbors, which can be other water molecules and/or OS molecules. The lower three diagrams show, vice versa, the centroid position of the partial molar Raman spectrum of the OS in the mixture with water and thus represent the development of the OS-HBN in the mixture. In this context, OS-HBN refers to the HBN that OS molecules develop with their neighbors, which can be other OS molecules and/or water molecules.

In the following paragraph we first describe in detail the behaviors of $\overline{\nu}^{OH}_{W(MeOH)}$ and $\overline{\nu}^{OH}_{MeOH(W)}$.

For pure water $x_w = 1$, it can be seen that $\overline{\nu}^{OH}_{W(MeOH)}$ and $\overline{\nu}^{OH}_{MeOH(W)}$ increase with increasing temperature. Thus, the water-HBN and the OS-HBN develop less with increasing temperature.

For molar fractions $1 > x_W > 0.8$ (regime 1) $\overline{\nu}^{OH}_{W(MeOH)}$ decreases to a minimum at $x_W \approx 0.8$, when pure water is diluted with MeOH. This means that in regime 1 the water-HBN develops stronger when more MeOH is added to the mixture until a maximum is reached at $x_W \approx 0.8$. On the contrary, $\overline{\nu}^{OH}_{MeOH(W)}$ (lower diagram in Figure 6) increases in the same regime when MeOH is added to pure water to a maximum at $x_W \approx 0.8$. This implies that MeOH at $x_W \approx 0.8$ develops the fewest H-bonds with its neighbors. Obviously, the minimum of $\overline{\nu}^{OH}_{W(MeOH)}$ and the maximum of $\overline{\nu}^{OH}_{MeOH(W)}$ can be found with the same mixture composition $x_W \approx 0.8$, meaning that the maximum development of the water-HBN exists when the minimum development of the OS-HBN exists. These observations are in support of theories that suppose the formation of an intense water-HBN around OS molecules, where the OS molecules participate less in the HBN, the more intense the water-HBN growth. This development turns around in the composition regime 2 for molar fractions $0.8 > x_W > 0.2$. With the addition of more MeOH, $\overline{\nu}^{OH}_{W(MeOH)}$ increases and $\overline{\nu}^{OH}_{MeOH(W)}$ decreases. Therefore, the water-HBN develops less and the OS-HBN develops stronger in regime 2 with the addition of more MeOH. One explanation is that when more than $x_W \approx 0.8$ MeOH molecules are present in the mixture, their dissolution is no more accomplished by surrounding them with a strong water-HBN, but by integrating them into the HBN of the mixture. Therefore, the OS-HBN becomes more intense, while the water-HBN becomes less intense. At the left border of regime 2 for mixture compositions of $x_W \approx 0.2$, $\overline{\nu}^{OH}_{W(MeOH)}$ shows a local maximum while $\overline{\nu}^{OH}_{MeOH(W)}$ has already reached approximately the value that we also measured for pure MeOH $x_W = 0$. The local maximum of $\overline{\nu}^{OH}_{W(MeOH)}$ implies that at $x_W \approx 0.2$ water molecules develop the fewest H-bonds with their neighbors. Diluting the mixture with even more MeOH in regime 3, which covers the compositions $0.2 > x_W > 0.0$, shows that $\overline{\nu}^{OH}_{MeOH(W)}$ remains at a constant level, irrespective of the mixture composition. Thus, the development of the OS-HBN seems not to be influenced by the mixture composition in regime 3. This is different for $\overline{\nu}^{OH}_{W(MeOH)}$, whose course in regime 3 very much depends on the mixture composition and temperature. At 308 K, $\overline{\nu}^{OH}_{W(MeOH)}$ decreases with increasing MeOH content in the mixture. This indicates that the water molecules develop more H-bonds with their neighbors, when there is more MeOH in the mixture. As at the same time the OS-HBN remains unaltered, we speculate that in regime 3 water molecules tend to develop H-bonds preferentially with other water molecules and seem to avoid MeOH molecules. This interpretation is in agreement with the theory of the formation of water-rich and MeOH-rich sub-micro domains (nanostructured fluids) that were found in water/alcohol mixtures.[13,22,30] At 328 K, $\overline{\nu}^{OH}_{W(MeOH)}$ shows a local minimum at $x_W \approx 0.1$. Therefore, the accumulation of water molecules in water-rich sub-micro domains, in which the water molecules tend to develop H-bonds mainly with other water-molecules, has a maximum at $x_W \approx 0.1$. In mixtures that at 328 K are even richer in MeOH $0.1 > x_W > 0.0$, these nanodomains disintegrate again, which is represented by the increase of $\overline{\nu}^{OH}_{W(MeOH)}$ toward $x_W = 0$.

What has been described above for the mixture W/MeOH can be transferred directly to the mixture W/EtOH. Therefore, we skip the description of the mixture W/EtOH. Nonetheless, the mixture compositions at which transitions from regime 1 to regime 2 and from regime 2 to regime 3 occur are slightly different. For both systems W/MeOH and W/EtOH, the composition at which the transition from regime 1 to regime 2 occurs (local minima of $\overline{\nu}^{OH}_{W(MeOH)}$ and $\overline{\nu}^{OH}_{W(EtOH)}$) coincides with the composition range at which the binary systems feature the extremes of the molar excess enthalpy.

In the mixture W/Acn the course of $\overline{\nu}^{OH}_{W(Acn)}$ as a function of the mixture composition is very different compared to the mixtures W/MeOH and W/EtOH. When diluting water with Acn, $\overline{\nu}^{OH}_{W(Acn)}$ increases monotonically. Therefore, the water-HBN is weakened more, when more Acn is added to the mixture. Putting this observation into context of the known existence of water-rich and Acn-rich clusters for mixture compositions $0.4 < x_W < 0.8$,[29,60] we can conclude that the water-HBN in the water-rich clusters are less developed than in pure water. It has been mentioned already above that the partial molar Raman spectrum of Acn contains an OH Raman signal, though the Acn molecule does not feature an OH vibration. This is due to the fact that partial molar properties show how the molar property of a mixture changes when infinitesimal amounts of Acn are added to the mixture. Thus, the partial molar Raman spectrum of Acn shows how the OH Raman signal of the mixture is influenced when the mixture is diluted with Acn. In this context, large values of $\overline{\nu}^{OH}_{Acn(W)}$ imply that Acn interacts with water molecules that develop a less intense HBN and small values of $\overline{\nu}^{OH}_{Acn(W)}$ imply that Acn interacts with water molecules that develop an intense HBN.

DOI: 10.1021/acs.jpcb.9b02829
J. Phys. Chem. B 2019, 123, 4425−4433

5. CONCLUSIONS

We here showed some insight into the mixtures of water and OSs that are based on the consideration of partial molar Raman spectra. The idea behind partial molar Raman spectra is identical to the concept of partial molar thermodynamic properties such as partial molar volume, enthalpy, entropy, energy, and others, but in our case only applied to Raman spectra.

Figure 6 and what has been discussed in its context show that information can be extracted from partial molar Raman spectra that is not extractable from mixture Raman spectra. The consideration of partial molar Raman spectra of water and of the OS made possible the analysis of the HBN that water molecules develop with their neighbors and that OS molecules develop with their neighbors. Because of this, for the mixtures water/methanol and water/ethanol we found three different regimes, in which the interaction mechanisms between water and alcohol change.

In general, the computation of partial molar Raman spectra is not limited to binary mixtures. However, more the constituents present in the mixture, more the experimental Raman spectra have to be determined in order to compute the partial molar Raman spectra of each compound.

What we showed for the HBN is possible for any intermolecular interaction that modulates a signal peak in the Raman spectra. We carried out these experiments at a pressure of 0.4 MPa, as some pressure is required to obtain reproducible operational conditions in the MCS. Due to the low compressibility of the binary systems analyzed, we speculate that the binary systems at ambient pressure would show very similar results.

■ ASSOCIATED CONTENT

Supporting Information

The Supporting Information is available free of charge on the ACS Publications website at DOI: 10.1021/acs.jpcb.9b02829.

Detailed description of the chain of processing the spectra and a list of analyzed mixture compositions with their measured densities (PDF)

■ AUTHOR INFORMATION

Corresponding Author

*E-mail: andreas.braeuer@tu-freiberg.de.

ORCID

Simon Stehle: 0000-0002-7112-695X

Andreas Siegfried Braeuer: 0000-0002-7816-4027

Author Contributions

The manuscript was written through contributions of all authors. All authors have given approval to the final version of the manuscript.

Notes

The authors declare no competing financial interest.

■ ACKNOWLEDGMENTS

The project leading to this contribution has received funding from the European Union's Horizon 2020 research and innovation programme under grant agreement no. 637654 (Inhomogeneities). The authors also gratefully acknowledge the funding of Erlangen Graduate School in Advanced Optical Technologies (SAOT) by the German Research Foundation (DFG) in the framework of the German excellence initiative.

■ REFERENCES

(1) Frank, H. S.; Evans, M. W. Free Volume and Entropy in Condensed Systems III. Entropy in Binary Liquid Mixtures; Partial Molal Entropy in Dilute Solutions; Structure and Thermodynamics in Aqueous Electrolytes. *J. Chem. Phys.* **1945**, *13*, 507−532.

(2) Titantah, J. T.; Karttunen, M. Long-Time Correlations and Hydrophobe-Modified Hydrogen-Bonding Dynamics in Hydrophobic Hydration. *J. Am. Chem. Soc.* **2012**, *134*, 9362−9368.

(3) Straatsma, T. P.; Berendsen, H. J. C.; Postma, J. P. M. Free Energy of Hydrophobic Hydration: A Molecular Dynamics Study of Noble Gases in Water. *J. Chem. Phys.* **1986**, *85*, 6720−6727.

(4) Tan, M.-L.; Miller, B. T.; Te, J.; Cendagorta, J. R.; Brooks, B. R.; Ichiye, T. Hydrophobic Hydration and the Anomalous Partial Molar Volumes in Ethanol-Water Mixtures. *J. Chem. Phys.* **2015**, *142*, 064501.

(5) Pangali, C.; Rao, M.; Berne, B. J. Hydrophobic Hydration around a Pair of Apolar Species in Water. *J. Solution Chem.* **1979**, *71*, 2982.

(6) Blokzijl, W.; Engberts, J. B. F. N. Hydrophobic Effects. Opinions and Facts. *Angew. Chem., Int. Ed. Engl.* **1993**, *32*, 1545−1579.

(7) Dolenko, T.; Burikov, S.; Hojo, M.; Patsaeva, S.; Yuzhakov, V. Hydrogen Bonding in Aqueous Ethanol Solutions Studied by Raman Spectroscopy. *Laser Appl. in Life Sci.* **2010**, *7376*, 73761B.

(8) Rezus, Y. L. A.; Bakker, H. J. Observation of Immobilized Water Molecules around Hydrophobic Groups. *Phys. Rev. Lett.* **2007**, *99*, 148301.

(9) Galamba, N. Water's Structure around Hydrophobic Solutes and the Iceberg Model. *J. Phys. Chem. B* **2013**, *117*, 2153−2159.

(10) Grdadolnik, J.; Merzel, F.; Avbelj, F. Origin of Hydrophobicity and Enhanced Water Hydrogen Bond Strength near purely Hydrophobic Solutes. *Proc. Natl. Acad. Sci. U.S.A.* **2017**, *114*, 322−327.

(11) Dolenko, T. A.; Burikov, S. A.; Dolenko, S. A.; Efitorov, A. O.; Plastinin, I. V.; Yuzhakov, V. I.; Patsaeva, S. V. Raman Spectroscopy of Water-Ethanol Solutions: The Estimation of Hydrogen Bonding Energy and the Appearance of Clathrate-like Structures in Solutions. *J. Phys. Chem. A* **2015**, *119*, 10806−10815.

(12) Gill, S. J.; Dec, S. F.; Olofsson, G.; Wadsoe, I. Anomalous Heat Capacity of Hydrophobic Solvation. *J. Phys. Chem.* **1985**, *89*, 3758−3761.

(13) Benson, S. P.; Pleiss, J. Incomplete Mixing versus Clathrate-like Structures: A Molecular View on Hydrophobicity in Methanol-Water Mixtures. *J. Mol. Model.* **2013**, *19*, 3427−3436.

(14) Chandler, D. Interfaces and the Driving Force of Hydrophobic Assembly. *Nature* **2005**, *437*, 640−647.

(15) Dougan, L.; Hargreaves, R.; Bates, S. P.; Finney, J. L.; Réat, V.; Soper, A. K.; Crain, J. Segregation in Aqueous Methanol Enhanced by Cooling and Compression. *J. Chem. Phys.* **2005**, *122*, 174514.

(16) Laage, D.; Stirnemann, G.; Hynes, J. T. Why Water Reorientation slows without Iceberg Formation around Hydrophobic Solutes. *J. Phys. Chem. B* **2009**, *113*, 2428−2435.

(17) Dixit, S.; Crain, J.; Poon, W. C. K.; Finney, J. L.; Soper, A. K. Molecular Segregation Observed in a Concentrated Alcohol-Water Solution. *Nature* **2002**, *416*, 829−832.

(18) Guo, J.-H.; Luo, Y.; Augustsson, A.; Kashtanov, S.; Rubensson, J.-E.; Shuh, D. K.; Agren, H.; Nordgren, J. Molecular Structure of Alcohol-Water Mixtures. *Phys. Rev. Lett.* **2003**, *91*, 157401.

(19) Moreau, C.; Douhéret, G. Thermodynamic and Physical Behaviour of Water + Acetonitrile Mixtures. Dielectric Properties. *J. Chem. Thermodyn.* **1976**, *8*, 403−410.

(20) Jamroz, D.; Stangret, J.; Lindgren, J. An Infrared Spectroscopic Study of the Preferential Solvation in Water-Acetonitrile Mixtures. *J. Am. Chem. Soc.* **1993**, *115*, 6165−6168.

(21) Bertie, J. E.; Lan, Z. Liquid Water−Acetonitrile Mixtures at 25 °C: The Hydrogen-Bonded Structure Studied through Infrared Absolute Integrated Absorption Intensities. *J. Phys. Chem. B* **1997**, *101*, 4111−4119.

(22) Chen, J.; Sit, P. H.-L. Ab Initio Study of the Structural Properties of Acetonitrile−Water Mixtures. *Chem. Phys.* **2015**, *457*, 87−97.

DOI: 10.1021/acs.jpcb.9b02829
J. Phys. Chem. B 2019, 123, 4425−4433

(23) Bakker, H. J. Physical Chemistry: Water's Response to the Fear of Water. *Nature* **2012**, *491*, 533−535.
(24) Davis, J. G.; Gierszal, K. P.; Wang, P.; Ben-Amotz, D. Water Structural Transformation at Molecular Hydrophobic Interfaces. *Nature* **2012**, *491*, 582−585.
(25) Idrissi, A.; Longelin, S.; Sokolić, F. Study of Aqueous Acetone Solution at Various Concentrations: Low-Frequency Raman and Molecular Dynamics Simulations. *J. Phys. Chem. B* **2001**, *105*, 6004−6009.
(26) Kovacs, H.; Laaksonen, A. Molecular Dynamics Simulation and NMR Study of Water-Acetonitrile Mixtures. *J. Am. Chem. Soc.* **1991**, *113*, 5596−5605.
(27) Marcus, Y.; Migron, Y. Polarity, Hydrogen Bonding, and Structure of Mixtures of Water and Cyanomethane. *J. Phys. Chem.* **1991**, *95*, 400−406.
(28) Byakov, V. M.; Lanshina, L. V.; Stepanova, O. P.; Stepanov, S. V. The Nanoheterogeneous Structure of Aqueous Solutions of n-Propanol. *Russ. J. Phys. Chem.* **2009**, *83*, 214−219.
(29) Takamuku, T.; Tabata, M.; Yamaguchi, A.; Nishimoto, J.; Kumamoto, M.; Wakita, H.; Yamaguchi, T. Liquid Structure of Acetonitrile−Water Mixtures by X-ray Diffraction and Infrared Spectroscopy. *J. Phys. Chem. B* **1998**, *102*, 8880−8888.
(30) Li, R.; D'Agostino, C.; McGregor, J.; Mantle, M. D.; Zeitler, J. A.; Gladden, L. F. Mesoscopic Structuring and Dynamics of Alcohol/Water Solutions probed by Terahertz Time-domain Spectroscopy and pulsed Field Gradient Nuclear Magnetic Resonance. *J. Phys. Chem. B* **2014**, *118*, 10156−10166.
(31) Lin, K.; Hu, N.; Zhou, X.; Liu, S.; Luo, Y. Reorientation Dynamics in Liquid Alcohols from Raman Spectroscopy. *J. Raman Spectrosc.* **2012**, *43*, 82−88.
(32) Hands, M. D.; Slipchenko, L. V. Intermolecular Interactions in Complex Liquids: Effective Fragment Potential Investigation of Water-tert-Butanol Mixtures. *J. Phys. Chem. B* **2012**, *116*, 2775−2786.
(33) Subramanian, D.; Anisimov, M. A. Phase Behavior and Mesoscale Solubilization in Aqueous Solutions of Hydrotropes. *Fluid Phase Equilib.* **2014**, *362*, 170−176.
(34) Venables, D. S.; Schmuttenmaer, C. A. Spectroscopy and Dynamics of Mixtures of Water with Acetone, Acetonitrile, and Methanol. *J. Chem. Phys.* **2000**, *113*, 11222−11236.
(35) Bergman, D. L.; Laaksonen, A. Topological and Spatial Structure in the Liquid-Water−Acetonitrile Mixture. *Phys. Rev. E: Stat. Phys., Plasmas, Fluids, Relat. Interdiscip. Top.* **1998**, *58*, 4706−4715.
(36) Mountain, R. D. Microstructure and Hydrogen Bonding in Water-Acetonitrile Mixtures. *J. Phys. Chem. B* **2010**, *114*, 16460−16464.
(37) Dougan, L.; Bates, S. P.; Hargreaves, R.; Fox, J. P.; Crain, J.; Finney, J. L.; Réat, V.; Soper, A. K. Methanol-Water Solutions: A bi-Percolating Liquid Mixture. *J. Chem. Phys.* **2004**, *121*, 6456−6462.
(38) Egashira, K.; Nishi, N. Low-Frequency Raman Spectroscopy of Ethanol−Water Binary Solution: Evidence for Self-Association of Solute and Solvent Molecules. *J. Phys. Chem. B* **1998**, *102*, 4054−4057.
(39) Cringus, D.; Yeremenko, S.; Pshenichnikov, M. S.; Wiersma, D. A. Hydrogen Bonding and Vibrational Energy Relaxation in Water−Acetonitrile Mixtures. *J. Phys. Chem. B* **2004**, *108*, 10376−10387.
(40) Mountain, R. D. Molecular Dynamics Study of Water−Acetonitrile Mixtures. *J. Phys. Chem. A* **1999**, *103*, 10744−10748.
(41) Noskov, S. Y.; Lamoureux, G.; Roux, B. Molecular Dynamics Study of Hydration in Ethanol-Water Mixtures using a Polarizable Force Field. *J. Phys. Chem. B* **2005**, *109*, 6705−6713.
(42) Wakisaka, A.; Matsuura, K. Microheterogeneity of Ethanol−Water Binary Mixtures Observed at the Cluster Level. *J. Mol. Liq.* **2006**, *129*, 25−32.
(43) Soper, A. K.; Dougan, L.; Crain, J.; Finney, J. L. Excess Entropy in Alcohol-Water Solutions: A Simple Clustering Explanation. *J. Phys. Chem. B* **2006**, *110*, 3472−3476.
(44) Bakó, I.; Megyes, T.; Grósz, T.; Pálinkás, G.; Dore, J. Structural Investigation of Water−Acetonitrile Mixtures: Small-Angle and Wide-Angle Neutron Diffraction Study Compared to Molecular Dynamics Simulation. *J. Mol. Liq.* **2006**, *125*, 174−180.
(45) Maréchal, Y.. *The Hydrogen Bond and the Water Molecule*; Elsevier, 2007.
(46) Nedić, M.; Wassermann, T. N.; Larsen, R. W.; Suhm, M. A. A Combined Raman- and Infrared Jet Study of Mixed Methanol-Water and Ethanol-Water Clusters. *Phys. Chem. Chem. Phys.* **2011**, *13*, 14050−14063.
(47) Koga, Y.; Sebe, F.; Minami, T.; Otake, K.; Saitow, K.-i.; Nishikawa, K. Spectrum of Excess Partial Molar Absorptivity. I. Near Infrared Spectroscopic Study of Aqueous Acetonitrile and Acetone. *J. Phys. Chem. B* **2009**, *113*, 11928−11935.
(48) Li, Q.; Wang, N.; Zhou, Q.; Sun, S.; Yu, Z. Excess Infrared Absorption Spectroscopy and its Applications in the Studies of Hydrogen Bonds in Alcohol-containing Binary Mixtures. *Appl. Spectrosc.* **2008**, *62*, 166−170.
(49) Wallace, V. M.; Dhumal, N. R.; Zehentbauer, F. M.; Kim, H. J.; Kiefer, J. Revisiting the Aqueous Solutions of Dimethyl Sulfoxide by Spectroscopy in the Mid- and Near-Infrared: Experiments and Car-Parrinello Simulations. *J. Phys. Chem. B* **2015**, *119*, 14780−14789.
(50) Takebayashi, Y.; Mashimo, Y.; Koike, D.; Yoda, S.; Furuya, T.; Sagisaka, M.; Otake, K.; Sakai, H.; Abe, M. Fourier Transform Infrared Spectroscopic Study of Water-in-Supercritical CO2 Microemulsion as a Function of Water Content. *J. Phys. Chem. B* **2008**, *112*, 8943−8949.
(51) Burikov, S.; Dolenko, S.; Dolenko, T.; Patsaeva, S.; Yuzhakov, V. Decomposition of Water Raman Stretching Band with a Combination of Optimization Methods. *Mol. Phys.* **2010**, *108*, 739−747.
(52) Dolenko, T. A.; Burikov, S. A.; Patsaeva, S. V.; Yuzhakov, V. I. Manifestation of Hydrogen Bonds of Aqueous Ethanol Solutions in the Raman Scattering Spectra. *Quantum Electron.* **2011**, *41*, 267−272.
(53) Fukasawa, T.; Amo, Y.; Tominaga, Y. Low-Frequency Raman Scattering Study of tert -Butyl Alcohol−Water and Tetrahydrofuran−Water Binary Mixtures. *J. Chem. Phys.* **2003**, *118*, 6387−6393.
(54) Grimaldi, N.; Rojas, P. E.; Stehle, S.; Cordoba, A.; Schweins, R.; Sala, S.; Luelsdorf, S.; Piña, D.; Veciana, J.; Faraudo, J.; et al. Pressure-Responsive, Surfactant-Free CO2-Based Nanostructured Fluids. *ACS Nano* **2017**, *11*, 10774.
(55) Cunningham, G. P.; Vidulich, G. A.; Kay, R. L. Several Properties of Acetonitrile-Water, Acetonitrile-Methanol, and Ethylene Carbonate-Water Systems. *J. Chem. Eng. Data* **1967**, *12*, 336−337.
(56) Armitage, D. A.; Blandamer, M. J.; Foster, M. J.; Hidden, N. J.; Morcom, K. W.; Symons, M. C. R.; Wootten, M. J. Thermodynamic, Ultrasonic, Spectroscopic and Miscibility Studies of Water + Methyl Cyanide Solutions. *Trans. Faraday Soc.* **1968**, *64*, 1193.
(57) Davis, M. I. Analyses of Excess Molar Volumes of the Acetonitrile-Water System using Segmented Composition Models. *Thermochim. Acta* **1983**, *71*, 59−78.
(58) Stokes, R. H. Excess Partial Molar Enthalpies for (Acetonitrile + Water) from 278 to 318 K. *J. Chem. Thermodyn.* **1987**, *19*, 977−983.
(59) Schneider, G. Druckeinfluß auf die Entmischung flüssiger Systeme. *Z. Phys. Chem.* **1964**, *41*, 327−338.
(60) Takamuku, T.; Yamaguchi, A.; Matsuo, D.; Tabata, M.; Kumamoto, M.; Nishimoto, J.; Yoshida, K.; Yamaguchi, T.; Nagao, M.; Otomo, T.; et al. Large-Angle X-ray Scattering and Small-Angle Neutron Scattering Study on Phase Separation of Acetonitrile−Water Mixtures by Addition of NaCl. *J. Phys. Chem. B* **2001**, *105*, 6236−6245.

DOI: 10.1021/acs.jpcb.9b02829
J. Phys. Chem. B 2019, 123, 4425−4433